Global and Planetary Change 129 (2015) 56–68

Contents lists available at ScienceDirect

Global and Planetary Change

journal homepage: www.elsevier.com/locate/gloplacha

Increased precipitation drives mega slump development and destabilization of ice-rich permafrost terrain, northwestern Canada

S.V. Kokelj [a,*], J. Tunnicliffe [b], D. Lacelle [c], T.C. Lantz [d], K.S. Chin [e], R. Fraser [f]

[a] Northwest Territories Geological Survey, Industry, Tourism and Investment, Government of the Northwest Territories, Yellowknife, NT Canada
[b] School of Environment, University of Auckland, Auckland, New Zealand
[c] Department of Geography, University of Ottawa, Ottawa, ON Canada
[d] School of Environmental Studies, University of Victoria, Victoria, BC Canada
[e] Cumulative Impact Monitoring Program, Environment and Natural Resources, Government of the Northwest Territories, Yellowknife, NT Canada
[f] Canada Centre for Remote Sensing, Natural Resources Canada, Ottawa, ON Canada

ARTICLE INFO

Article history:
Received 19 August 2014
Received in revised form 15 February 2015
Accepted 22 February 2015
Available online 28 February 2015

Keywords:
climate change
ground ice
landscape change
mass wasting
permafrost
rainfall intensity
thaw slump
thermokarst

ABSTRACT

It is anticipated that an increase in rainfall will have significant impacts on the geomorphology of permafrost landscapes. Field observations, remote sensing and historical climate data were used to investigate the drivers, processes and feedbacks that perpetuate the growth of large retrogressive thaw slumps. These "mega slumps" (5–40 ha) are now common in formerly glaciated, fluvially incised, ice-cored terrain of the Peel Plateau, NW Canada. Individual thaw slumps can persist for decades and their enlargement due to ground ice thaw can displace up to 10^6 m^3 of materials from slopes to valley bottoms reconfiguring slope morphology and drainage networks. Analysis of Landsat images (1985–2011) indicate that the number and size of active slumps and debris tongue deposits has increased significantly with the recent intensification of rainfall. The analyses of high resolution climatic and photographic time-series for summers 2010 and 2012 shows strong linkages amongst temperature, precipitation and the downslope sediment flux from active slumps. Ground ice thaw supplies meltwater and sediments to the slump scar zone and drives diurnal pulses of surficial flow. Coherence in the timing of down valley debris tongue deposition and fine-scaled observations of sediment flux indicate that heavy rainfall stimulates major mass flow events. Evacuation of sediments from the slump scar zone can help to maintain a headwall of exposed ground ice, perpetuating slump growth and leading to larger disturbances. The development of debris tongue deposits divert streams and increase thermoerosion to initiate adjacent slumps. We conclude that higher rainfall can intensify thaw slump activity and rapidly alter the slope-sediment cascade in regions of ice-cored glaciogenic deposits.

1. Introduction

Increases in air temperature and precipitation at high latitudes have the potential to dramatically alter ice-rich permafrost landscapes. Late 20th Century climate warming has caused permafrost temperatures to increase (Romanovsky et al., 2010) and thermokarst activity to intensify (Kokelj and Jorgenson, 2013). Numerical models of the cryosphere energy balance that incorporate climate projections forecast the widespread degradation of near-surface permafrost over the next century (Callaghan et al., 2011). Global circulation models also predict significant increases in high latitude precipitation and extreme rainfall events (Walsh et al., 2011). A greater frequency and magnitude of rainfall events can influence the geomorphic evolution of permafrost landscapes by: i) increasing sensible heat transfer and the latent heat content of soils, which may slow the freezeback of the active layer and cause the permafrost to warm (Kokelj et al., 2014); ii) increasing slope sediment and solute yields (Lewkowicz and Kokelj, 2002; Lafrenière and Lamoureux, 2013); iii) accelerating thermoerosion, which can cause gullying (Fortier et al., 2007) and river bank destabilization; and iv) increasing the potential of slope instability (McRoberts and Morgenstern, 1974; Lewkowicz and Harris, 2005; Lacelle et al., 2010). To date, very few process-oriented studies have documented the impacts of rainfall on slope stability and mass wasting in continuous permafrost terrain (Cogley and McCann, 1976; Lamoureux and Lafrenière, 2009).

Retrogressive thaw slumps are a common form of thermokarst in areas of ice-rich glaciogenic deposits, including the Peel Plateau of northwestern Canada (Figs. 1 and 2) (Lacelle et al., 2010; Brooker et al., 2014). Active thaw slumps are comprised of an ice-rich headwall, a low-angled scar zone consisting of thawed slurry and in some cases a periodically mobile tongue of debris that develops as the saturated materials flow downslope (Fig. 2) (Burn and Lewkowicz, 1990). Surface energy fluxes, ground ice and headwall characteristics (size and

* Corresponding author at: Northwest Territories Geological Survey, P.O. Box 1320, Yellowknife, NT, X1A 2L9, Canada. Tel.: +1 867 765 6610.
E-mail address: Steve_Kokelj@gov.nt.ca (S.V. Kokelj).

http://dx.doi.org/10.1016/j.gloplacha.2015.02.008

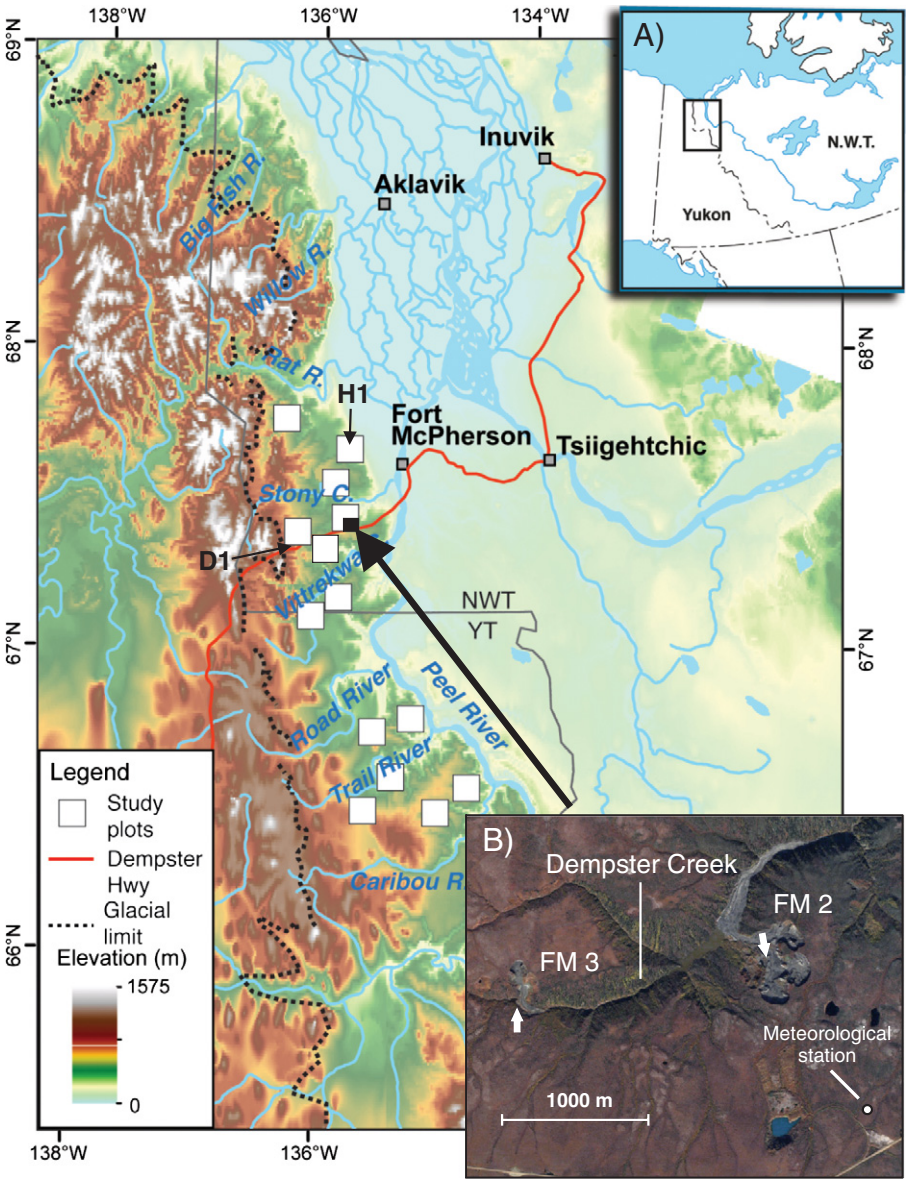

Fig. 1. Map showing Peel Plateau study region and 14 Landsat study plots where active slump and debris tongue surfaces were mapped. Inset A shows the location of the study area within NW Canada. Inset B shows slumps FM2 and FM3, the meteorological station and the white arrows show location and orientations of the monitoring cameras.

orientation) control the headwall ablation rate (Lewkowicz, 1987; Grom and Pollard, 2008; Lacelle et al., 2015) and gravity-driven flows move debris and meltwater to the base of the headwall. The thawed materials can be transported from the slump headwall by rill erosion, fluvial transport and shallow and deep-seated mass flows (Murton, 2001; Lacelle et al., 2010; Lantuit et al., 2012). Although these processes have received little attention in past investigations, evacuation of debris from the slump scar zone is a key factor determining whether a slump remains active or stabilizes.

In the Peel Plateau region, high relief of the fluvially incised, ice-rich landscape provides sufficient transport gradient to evacuate slumped materials, promoting the development of large slumps and debris tongue deposits (Fig. 2) (Kokelj et al., 2013; Brooker et al., 2014). This terrain is similar to many other fluvially incised, ice-cored, glaciogenic landscapes in North America (St-Onge and McMartin, 1999; Jorgenson et al., 2008; Lakeman and England, 2012) and Siberia (Astakhov et al., 1996; Alexanderson et al., 2002). As thaw slumps enlarge to several hectares in area they tend to exhibit greater geomorphic complexity, including different modes of downslope sediment displacement, which operate across a range of temporal and spatial scales. The processes and characteristics associated with these "mega slumps" include: (1) exposure of, and ablation of, large massive ice bodies, backwasting of the headwall by retrogressive failure and supply of sediments and meltwater to a low-angled scar zone (Fig. 2); (2) evacuation of debris from the scar zone proceeding as a complex combination of fluvial transport, intermittent mass wasting (gravitational collapse, slumps, torrents, debris flow), and quasi-continuous fluidized mass flow (Lacelle et al., 2010; Lantuit et al., 2012; Kokelj et al., 2013); (3) base-level erosion, or evacuation of outlet detritus, (4) prolonged slump activity over decades producing disturbances that grow to tens of hectares area (Brooker et al., 2014); and (5) valley-confined downstream aggradation of debris derived from the scar zone, leading to cascading effects including development of debris dammed lakes and enhanced valley-side erosion (Fig. 2F, G).

There is growing field evidence to suggest that slump activity has recently intensified across a range of Arctic landscapes (Lantuit and Pollard, 2008; Lantz and Kokelj, 2008), but the linkages between climatic drivers and development of larger slumps remains poorly understood (Kokelj and Jorgenson, 2013). Our primary objectives are to determine if thaw slumping has increased in the Peel Plateau region, and to

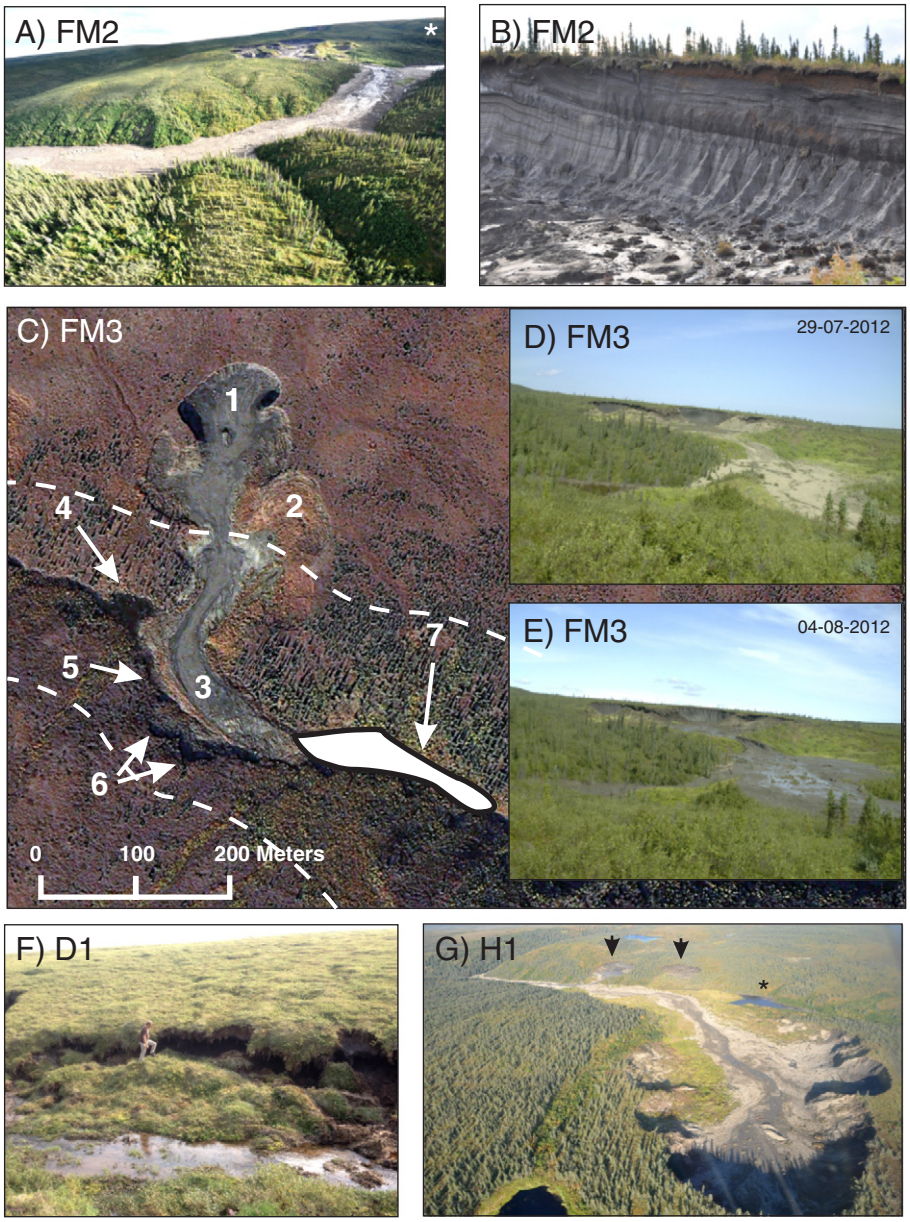

Fig. 2. Thaw slumps in the Peel Plateau. A) Slump FM2 and debris tongue. The debris tongue is 1.5 km in length and total disturbed area in 2011 was about 38 ha. The asterisk indicates a debris dammed lake. B) The headwall of slump FM2 showing banded massive ice overlain by oxidized tills. This headwall is approximately 25 m high. C) Quickbird image from September, 2008 of thaw slump FM3, showing: 1) active scar area; 2) stable, vegetated scar; 3) debris tongue; 4) debris dammed pond; 5) diverted creek along valley side; 6) secondary thaw slumps; and 7) growth of debris tongue in summer 2010 and 2012. Dashed line indicates approximate location of the break in slope. D) Headwall, scar zone and upper debris tongue of slump FM3 prior to and E) following an extreme rainfall event (92 mm) from July 31–August 1, 2012. The July image (D) shows an actively ablating headwall, saturated soils in a low-angled scar zone and a rill system draining through debris tongue and (E) shows conditions during the mass flow event. F) Thermoerosion of a formerly stable slope and secondary slump initiation at D1 resulting from the diversion of a small creek by a debris tongue in the foreground. G) Secondary slumps associated with the slump and debris tongue at H1. Secondary slumps are indicated by black arrows and a debris dammed pond is indicated by the asterisk.

investigate the processes and feedbacks that influence slump activity. To achieve our first objective, we examined the linkages between air temperature, precipitation, and occurrence and activity of large slumps in the Peel Plateau using imagery from the Landsat archive (Fig. 1) and historical climate data. This regional component of our research was guided by the following hypotheses: (1) the upper size limit of thaw slumps and the geomorphic activity of these disturbed surfaces have recently increased; and (2) the evacuation of debris from the slump scar zone and the extents of debris tongue deposits have increased with summer rainfall.

In the second part of this paper, we used field observations and detailed monitoring of two particularly large slumps (FM2, FM3; Figs. 1, 2) in the Stony Creek watershed to refine our model of thaw slump mechanics. Specifically, we used time-lapse camera footage and meteorological instrumentation to assess the effects of diurnal and synoptic variables (radiative flux, temperature, precipitation) on the rate, intensity and modes of debris evacuation from the slump scar zone. The results are summarized in a simple conceptual model that links temperature, precipitation and sediment transport with the perpetuation of slump activity and growth of larger disturbances.

2. Field setting

The study area is in the Peel Plateau of northwestern Canada (Fig. 1). By about 18,000 ka yr BP this region was covered by the Laurentide Ice sheet, which extended to the eastern slopes of the Richardson Mountains (Lacelle et al., 2013) up to an elevation of 750 m a.s.l. The Peel Plateau consists of glaciogenic materials, predominantly

hummocky moraine (Duk-Rodkin and Hughes, 1992a,b), deposited along the retreating margins of the ice sheet to form a broad, gently eastward-sloping plateau with elevation ranging from 650 m in the Richardson Mountains to 100 m west of the Peel River, NWT (Catto, 1996). Deposits of similar glacial origin extend northward, at lower relief, through the Yukon coastal plain to Herschel Island and southward along the Mackenzie Mountains (Rampton, 1982; Fulton, 1995). The Peel Plateau consists of up to 60 m of glacial, glacio-fluvial, and glaciolacustrine sediments, overlying lower Cretaceous marine shale and siltstone bedrock (Norris, 1984). Colluviated materials veneer the valley slopes and alluvial deposits occupy the valley bottoms (Duk-Rodkin and Hughes, 1992a,b). The area is underlain by relatively warm (O'Neill et al., 2015), ice-rich permafrost (Lacelle et al., 2015). The depth to the base of permafrost is roughly 125 m (Mackay, 1967; Judge, 1973).

Eastward flowing streams from the Richardson Mountains have incised post-glacial valley networks that drain into the Peel River and the Mackenzie Delta (Fig. 1). The valleys are gently sloping in the highlands and the relative relief increases eastward, where several streams have carved deep, V-shaped valleys through the glacial deposits and the underlying sedimentary bedrock. Ice-rich permafrost and significant valley relief (up to 350 m) favour thaw slump development, which is restricted to the glaciogenic deposits at elevations of less than about 750 m a.s.l. (Brooker et al., 2014; Lacelle et al., 2015). Sediment samples from three thaw slumps in Willow River watershed (Bjornson, 2003) and from a large slump in our study area (FM3) (Fig. 1) consisted mainly of silts and clays (ca. 80%) with sands and gravels composing the remainder. The liquid limit and plasticity of the Willow River samples averaged 35% and 20%, respectively (Bjornson, 2003).

The regional climate is continental, with long cold winters and short cool summers. The mean annual air temperature at Fort McPherson (1986–2010) is −6.8 °C (Environment Canada, 2012). Mean July temperature is 15 °C, and the coldest month, January, has a mean temperature of −27 °C. In the area, mean annual air temperatures have increased at a rate of 0.77 °C per decade since the 1970s, with the warming trend strongest for the winter months (Burn and Kokelj, 2009). Total annual precipitation at Fort McPherson (1986–2007) averages 295 mm, with rainfall accounting for approximately half (148 mm) (Environment Canada, 2012). Convective summer storms are common and rainfall at Fort McPherson has increased in recent years (Fig. 3).

3. Methodology

3.1. Regional changes in the size distribution of thaw slumps

To evaluate trends in thaw slump activity and debris tongue development across the Peel Plateau we used Landsat satellite imagery acquired over the past 25 years. We characterized active slump and debris tongue size in 2011 and between 1985–1990 in 14 intensively impacted study plots, each 100 km^2 (Fig. 1). Images from multiple years were also used to investigate the progressive growth of debris tongues. Cloud free (<10%), summer season Landsat images dating from 1985 to 2011 were compiled from the Glovis website (http://glovis.usgs.gov/) to produce a sequence of 8 to 14 images for each of the 14 study plots. The reflectance of bare soils contrasts with vegetated surfaces so that large (~>0.8 ha or 3-by-3 pixels), geomorphically-active slump surfaces free of vegetation, and active debris tongues are readily identifiable on these Landsat images. Scar zones and debris tongue deposits were digitized as separate objects using ArcGIS10 to provide estimates of the area of active disturbance surface in 2011 and in the period from 1985–1990. Since the earliest, high quality images for two of the 14 study plots were from 1990, a total of seven slumps from two plots were first mapped in 1990 rather than in 1985. These seven features were grouped with 34 slumps from the other 12 study plots mapped with 1985 images. This grouped dataset (1985–1990) of active slump and debris tongue size was compared with disturbance areas derived from 2011 imagery. To test for significant differences in mean disturbance area between the late 1980's and 2011 we used Welch's two-sample *t*-test. The timing of debris tongue development was investigated by digitizing a subset of these deposits in every year that had available imagery.

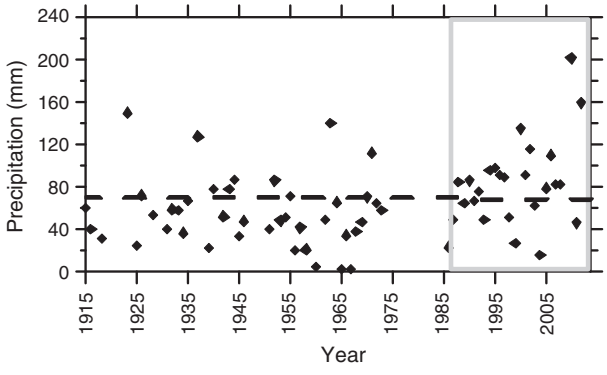

Fig. 3. Total June-July precipitation, at Fort McPherson, NWT. Mean rainfall for the entire period of record is indicated by the dashed line. The grey box indicates the time span covered by the available remote sensing data. (Environment Canada, 2012)

3.2. Historical climate and precipitation data, Fort McPherson, N.W.T.

To investigate linkages and feedbacks between hydroclimatic drivers and thaw slump activity, we compared trends in summer precipitation (1986–2012) and air temperature indices (1986–2010) from the Fort McPherson weather station (Environment Canada, 2012) with the timing of slump and debris tongue development derived from the Landsat images. Our analysis of trends in temperature indices was constrained to 2010 due to limited availability of data. However, it was possible to combine historical daily rainfall from Environment Canada (1986–2010) with unpublished data from the Fort McPherson airport (2010–2012), extending the precipitation record to 2012.

We examined annual trends in total June-July precipitation, thawing degree days, and number of days with temperature above 20 °C. We tested for trends in the time-series using the Mann-Kendall test, robust to missing values and serial dependence (Hirsch et al., 1982). Patterns in extreme rainfall events were summarized by tallying the number of daily events exceeding 15 mm, 20 mm and 25 mm in each year of record.

3.3. Field monitoring of active slumps: sediment transport index (STI)

To investigate finer-scale temporal patterns in the intensity of downslope sediment transport from a thaw slump scar zone, photo-monitoring stations with automated trail cameras (®Reconyx) were established within two large thaw slumps in the Peel Plateau in 2010 and 2012. One slump (FM2) was monitored in 2010 and two slumps (FM2 and FM3) were monitored in 2012 (Figs. 1B and 2). Each camera was mounted on a pipe anchored in the permafrost and positioned facing the slump headwall with a view of the scar zone debris field in the foreground. The cameras were programmed to take photographs at half hour intervals in 2010 and hourly intervals in 2012. We used two methods to derive indices of sediment transport activity and surface change using the photographic record. Throughout this paper we refer to these methods as: 1) the qualitative sediment transport index (STIa) and 2) the automated sediment transport index (STIb).

3.3.1. Sediment transport index a (STIa)

The photographic record was used to develop a semi-quantitative index of mass flow activity. This method was based on categorical variables that were visually assessed while comparing successive

photographs or sequences of several photographs. STIa was based on the following categories which were multiplied to give an hourly STI value.

$$\text{STIa} = \text{Downslope movement} * \text{width of movement} * \text{change in surface elevation} \quad (1)$$

(1) Downslope movement intensity: A score from 0 to 4 was assigned based on the relative rate of downslope movement (Fig. 4B). A value of 0 indicated that the mass flow was inactive and 4 represented maximum rate of downslope movement, which approached 100 m hr^{-1}, or the approximate length of mud flow run captured in the middle of the FM 2 image (Fig. 4).
(2) Width of active mass flow: A score from 1 to 4 was assigned based on the width of the downslope mass flow. A value of 1 was assigned when there was no movement and a value of 4 was recorded when the entire width of the mass flow in the central part of the image was showing at least some type of movement downslope. Intermediate categories (2: 1–30%; 3: 30–90%) were assigned according to the proportion of the feature's width that was actively transporting material. The maximum width of the active flow captured in the middle of the frame for FM2 was approximately 100 m (Fig. 4).
(3) Change in surface elevation and plug-like movement: Surface lowering of the scar zone and active flow surface was also assessed. During the most intense periods of mass wasting, deeper-seated, plug-like movement of the materials could lead to mobilization and lowering of the entire mass flow surface. A score from 1 to 4 was assigned based on the magnitude of this movement. A value of 1 indicated no surface lowering and a value of 4 indicated plug-like flow and significant surface lowering impacting the entire mass flow surface. The proportion of the disturbance that exhibited plug-like flow and surface lowering was used to assign intermediate categories (2: 1–30%; 3: 30–90%).

3.3.2. Sediment transport index b (STIb)

To support our qualitative index (STIa) for slump FM2 we developed an automated method to assess surface sediment movement within the camera's field of view, using the compositing capabilities of the open-source software ImageMagick® (v.6.8) to carry out grayscale differencing from one frame to the next. By 'subtracting' sequential raster images this process effectively highlights pixels where there have been changes in image brightness intensity to provide an index of surface change, and sediment transport activity (Fig. 4). The intensity of the differencing signal is a function of the total area undergoing surface change and the magnitude of transport activity. When large volumes of material are moving at high rates, differencing produces strongly contrasting images (Fig. 4C, D). A depth of field model for the camera's position was developed by creating approximate contour elevations of the slump, based on reference points from SPOT satellite imagery and field photos from the site (Fig. 4A). The pixels from the subtracted photo sequence were then multiplied by a distance factor to approximate the area weighting of each pixel (Fig. 4D). Motion from the rear of the field of view could then be sensibly added to motion in the foreground. The area represented by each pixel increases with the square of distance from the camera. In order to account for this perspective distortion the differenced imagery was multiplied by a weighting function:

$$\text{STIb} = \text{Diff} * \left(L^2\right) \Big/ \left(L_{max}{}^2\right) \quad (2)$$

where Diff = differencing intensity (0–255) and L is the modelled distance from the camera to the point on the terrain. L_{max} is the maximum

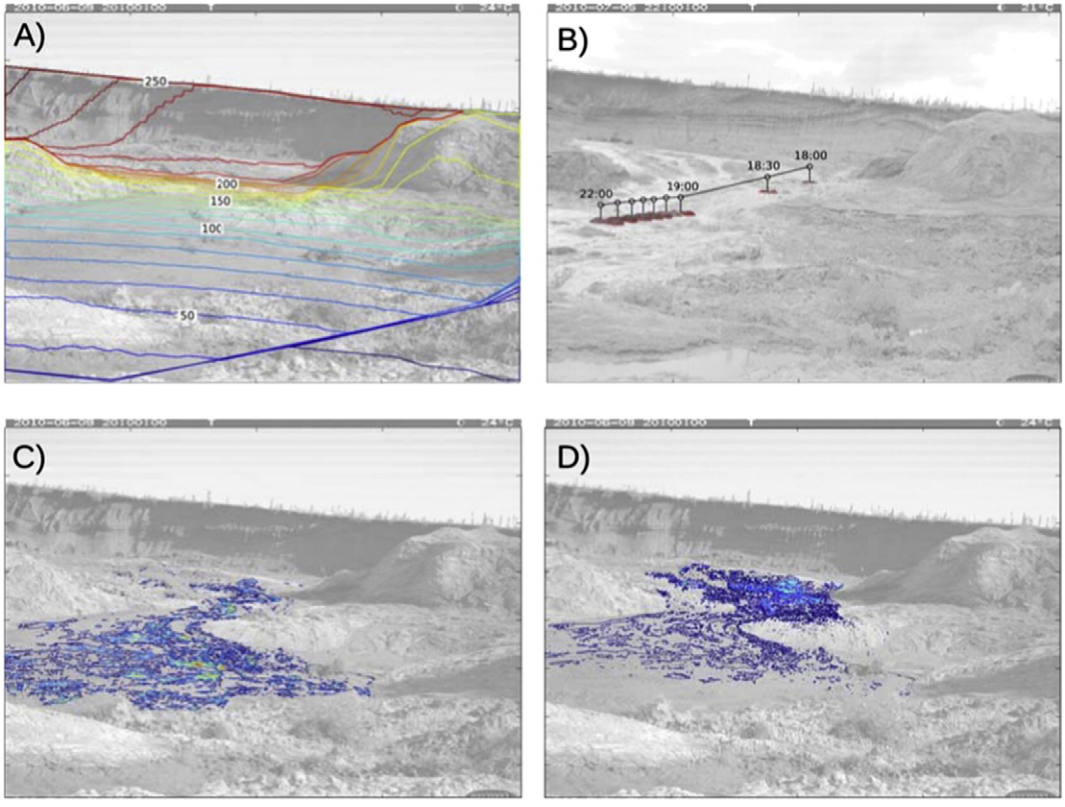

Fig. 4. A) Approximated depth map showing contours of terrain distance from camera, based on a digital elevation model and remote sensing imagery of the study area, slump FM2; B) Tracked movement of a single block of material within the mass flow, illustrating the variable velocity field for blocks of thaw slump detritus, July 5, 2010; C) Differencing intensity between two photos during a period of surficial fluvial reworking of the thaw slump surface materials; and D) Differencing map with distance weighting applied which provides more proportional representation of surface change in the rear field of view.

distance of geomorphic activity from the camera, 250 m in this case. For example, a pixel at 50 m was weighted at 0.04, one at 100 m was 0.16 and a pixel at the headwall (250 m) was weighted at 1.0. Using this technique, it was possible to automatically log the intensity of surface activity across the field of view (compare Fig. 4C and D), although manual editing was required to eliminate the obscuring influence of precipitation and morning or evening shadows.

3.3.2. Hydroclimate and STIa

To explore the relationships between mass flow and hydroclimatic drivers we examined correlations among STIa from slump FM2 and temperature and precipitation data from an automated meteorological station situated within 2 km of the two monitored slumps (Fig. 1B). The STIa was used in this analysis because the available record was longer than that generated by the automated method (STIb). However, the two time-series were significantly correlated ($r^2 = 0.45$; $p < 0.0001$) in 2010 as both captured similar diurnal and broader-scale temporal patterns in sediment movement. The meteorological station was established in June, 2010. Air temperature was measured using a YSI thermistor (44212) with a range from −50 °C to + 50 °C and an accuracy of ±0.1 °C. Rainfall was measured with a tipping bucket rain gauge (TE525M) with an accuracy of ±1% at precipitation rates up to 10 mm hr^{-1}, and an accuracy of ±5% at rates from 20 to 30 mm hr^{-1}. Net radiation was measured with a CNR2-L Net Radiometer which has a temperature dependant sensitivity of <5% from −10 °C to 40 °C. Meteorological data were logged at hourly intervals on a Campbell Scientific CR1000.

To explore the relationship between climate and sediment removal from the slump scar zone we used Spearman's rank correlation to measure covariance between STIa at FM2 and 1) total net radiation, 2) air temperature and 3) precipitation for 2010 and 2012. To determine if antecedent hydroclimate conditions influenced mass flow activity, we smoothed the climate data with back-cast running means of 0, 12, 24, 48 and 96 hours. Rainfall was smoothed using a running sum over the same back-looking window lengths. To examine if there were lags in the response of mass flow activity, we temporally shifted hydroclimate data by 0, 12, 48, 96 and 192 hours. Correlations between all combinations of smoothed and lagged hydroclimatic parameters and STIa were examined and the strongest relations are highlighted. To estimate the magnitude of mass flow activity before and after rainfall events, cumulative STIa, mean total net radiation and air temperature for 48 hour intervals preceding and following distinct rainfall events were also summarized. We only considered rainfall events greater than 10 mm that were preceded and followed by 48 hour periods with no rainfall (<2 mm). STIa before and after these rainfall events was compared using a paired *t*-test for 2010 and 2012 data. The STIa data for 2010 and 2012 were also summarized by three-week periods to investigate possible seasonal patterns in mass flow intensity.

4. Results

4.1. Intensification of thaw slump activity and debris tongue development, 1985—90 to 2011

The size distribution and abundance of large, active thaw slumps and mass flow surfaces shows a clear and pronounced increase from 1985–1990 to 2011 (Table 1; Figs. 5 and 6). The total number of large, geomorphically-active thaw slump surfaces visible on the 14 Landsat imagery study plots increased from 41 to 68 and the mean area increased significantly, from 3.8 ha in 1985–1990 to 9.9 ha in 2011 (Table 1; Fig. 5A). In 1985–1990 about 20% of the mapped slump surfaces were greater than 5.0 ha, but by 2011 approximately 60% of the active disturbance surfaces exceeded 5.0 ha and almost 20% were greater than 15 ha in area. Seven of the 41 features identified in 1985–1990 showed evidence of increased vegetation cover, suggesting that these slumps were stable or beginning to stabilize by 2011. The remainder of the 34 slumps identified in 1985–1990 continued to enlarge throughout the period of record, and an equal number (34) of additional active slump surfaces could be identified on the 2011 imagery.

Table 1
Summary statistics and Welch's two sample *t*-test comparing total disturbance, scar zone and debris tongue areas between the 1985–1990 and 2011 periods. Data is derived from Landsat imagery from 14 study plots each 100 km^2 in area. Minimum mappable disturbance area is 0.81 ha.

	Total disturbed area (ha)		Scar zone area (ha)		Debris tongue area (ha)	
	1985–1990	2011	1985–1990	2011	1985–1990	2011
Mean	3.84	9.87	2.84	6.88	3.19	6.61
Median	2.06	5.67	2.04	5.11	1.95	4.33
STDev	3.75	11.19	2.37	6.61	2.88	6.23
Maximum	17.30	66.80	12.70	40.10	9.89	26.20
Minimum	0.87	0.94	0.87	0.94	0.95	1.15
Count	41	68	40	67	14	31
t; df	4.047; 89.302		4.482; 91.096		2.463; 42.846	
Significance	P < 0.001		P < 0.0001		P = 0.0178	

The number and size of active debris tongue deposits in our study plots also increased significantly over the period of record (Table 1; Figs. 5B and 6). In the 1985–1990 period, a total of 14 mass flows with a mean area of 3.2 ha were identified downslope of slump scar zones. About half of the 68 slumps that were mapped in 2011 had clearly visible mass flow deposits with an average area of 6.6 ha (Table 1). The largest debris tongue mapped in 1985–1990 was 9.9 ha. The deposit had grown to 26.2 ha by 2011 and it had prograded several km down the main trunk valley.

4.2. Temperature and precipitation trends, 1986–2012

The increase in size and number of active disturbance surfaces has occurred in conjunction with the intensification of rainfall recorded at

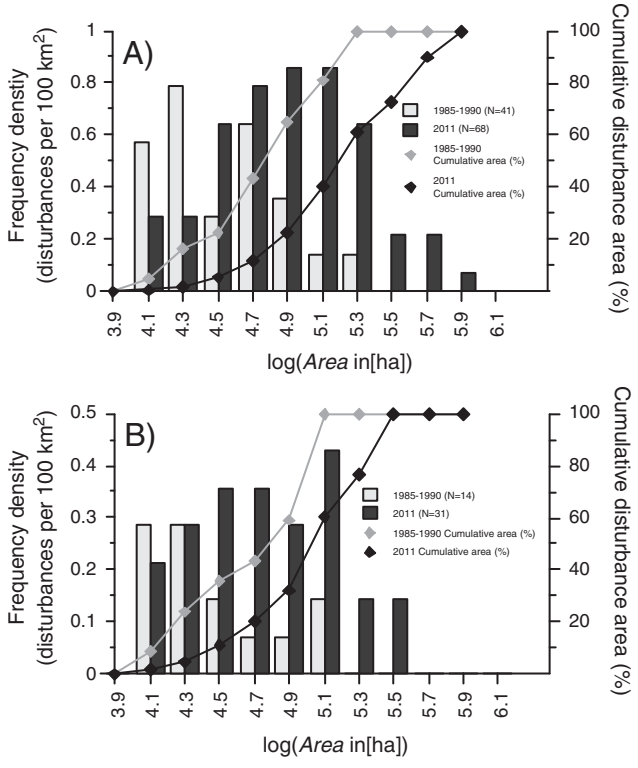

Fig. 5. A) Active slump surface; and B) debris tongue frequency density distribution and cumulative disturbance area for 1985–1990 and 2011. Data were derived from digitizing slump and debris tongue surfaces using Landsat imagery from 14(100 km^2) study plots for the respective time periods. Disturbances <0.81 ha were not mapped.

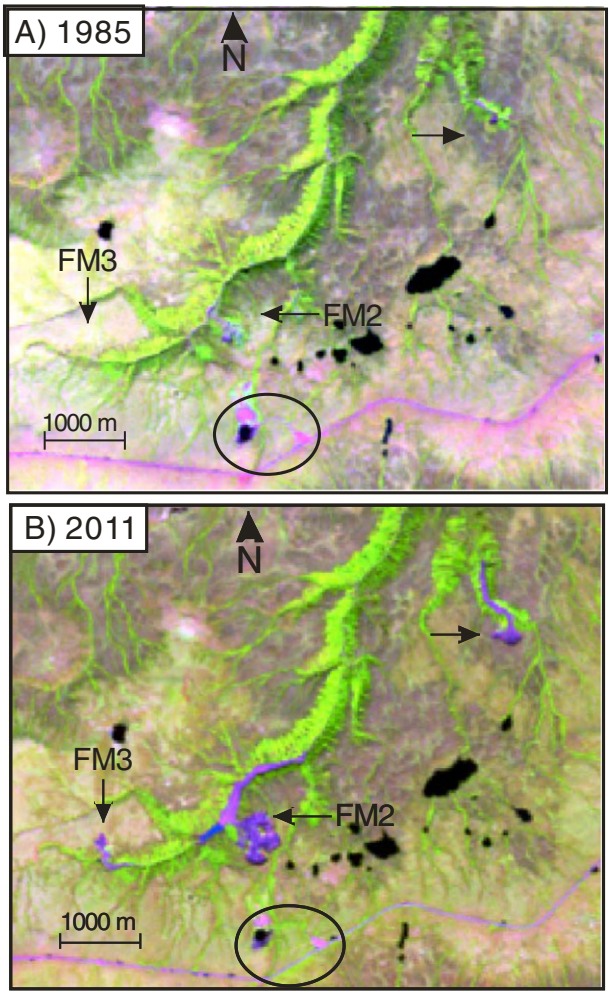

Fig. 6. Landsat images of the Peel Plateau from A) 1985 and B) 2011. The images are displayed as Landsat Ch5-Ch4-Ch3 = RGB. Unvegetated areas with bare soils are visible as blue, purple and pink. Several large slumps and debris tongues evident on the 2011 image are indicated by arrows. Most of these disturbances are smaller, partially vegetated or not visible on the 1985 imagery. Anthropogenic disturbances (quarries and roadside turnout) are indicated by the black circles. The Dempster Highway is also visible on the southern edge of both images.

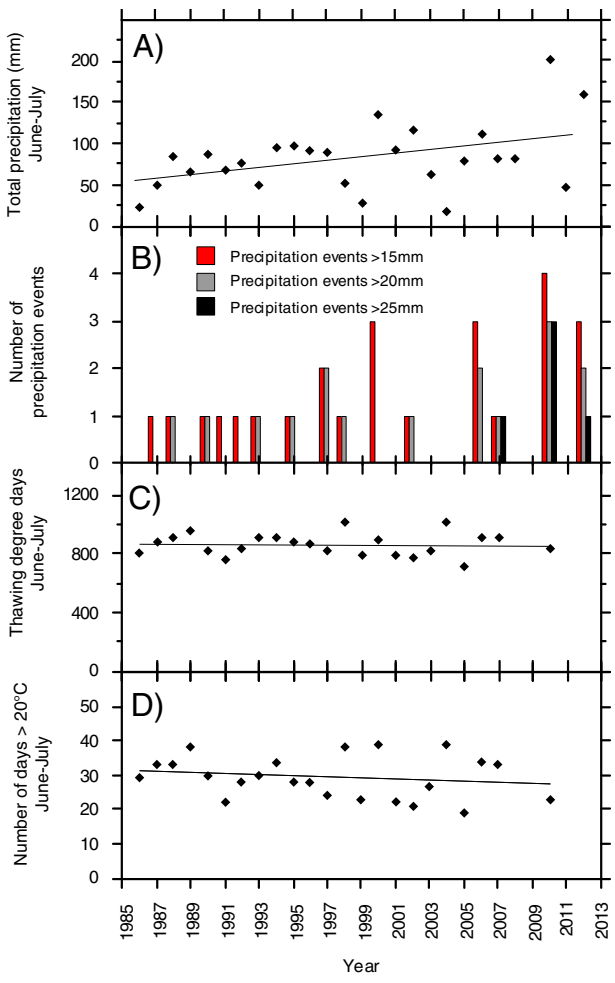

Fig. 7. Trends in precipitation and summer temperatures, 1986–2012, Fort McPherson, Northwest Territories, Canada. A) Total June–July precipitation. B) Number of extreme daily precipitation events in June and July. C) Thawing degree days in June and July. D) Number of days in June and July with maximum temperature exceeding 20 °C. Least squares linear regression curves are shown for plots A, C and D. The Mann-Kendall test indicates that only A) total June-July precipitation shows a significant (increasing) trend for the period of record.

Fort McPherson, NWT. Precipitation totals for June–July show that six of the ten wettest summers in an intermittent record extending back to 1915 have occurred since 1994, and 2010 and 2012 were the wettest two summers on record (Fig. 3). Climate data for the time period spanned by Landsat imagery (1985–2011) indicates a significant increase in total June–July rainfall ($\tau = 0.311$, $P < 0.05$) and a large increase in the frequency and magnitude of extreme rainfall events beginning around 2005 (Fig. 7A, B). The past decade has experienced the top five ranked daily rainfall events and the only ones to exceed 25 mm in the 1986–2012 period of record. These daily extremes include 40 mm and 64 mm events in 2010 and a 67 mm event in 2012. The gradual enlargement of several debris tongues rapidly accelerated after about 2005 and was coincident with an increase in the magnitude of rainfall events (Fig. 8). In contrast, the summer temperature related indices did not exhibit any significant trends during this period of increased slump and mass flow activity (Fig. 7C, D).

4.3. Feedbacks between debris tongue deposition and development of secondary slumps

Our field observations show that the growth of debris tongues that extend from the slump scar into the downstream valleys frequently obstructed lateral tributaries (Fig. 2A, C, G). This valley-filling can raise stream base-level at the confluence with the larger valley, leading to channel diversions and valley-side thermoerosion, exposure of ground ice and secondary thaw slump initiation (Fig. 2C, F, G). Between 1985 and 1990, 4 of the 41 active slump disturbance areas mapped in the study plots were a part of slump clusters that had developed around debris tongue deposits. Examination of the Landsat images from 1985 to 2011 revealed that the frequency of secondary slump occurrence closely followed the increased development of debris tongues (Fig. 9). On the 2011 Landsat images, well-developed secondary thaw slumps could be identified adjacent to 18 of the 31 debris tongue deposits visible on the study plots.

4.4. Slump descriptions and patterns in the sediment transport index, 2010 and 2012

4.4.1. Slump FM2, 2010 and 2012

In summer 2010 and 2012, thaw slump activity was monitored at FM2 (Fig. 1). At this site, intensive thaw slumping has exposed an ice-rich headwall about 1.4 km in length and between 3 and 25 m in height (Figs. 1 and 2B). The scar zone and debris tongue extended several hundreds of meters down a 3–10° slope. The disturbance has persisted, albeit as a much smaller, partially vegetated surface (Fig. 6), since at least 1954. By 2011 the scar zone and debris tongue had grown to 23.4 ha and

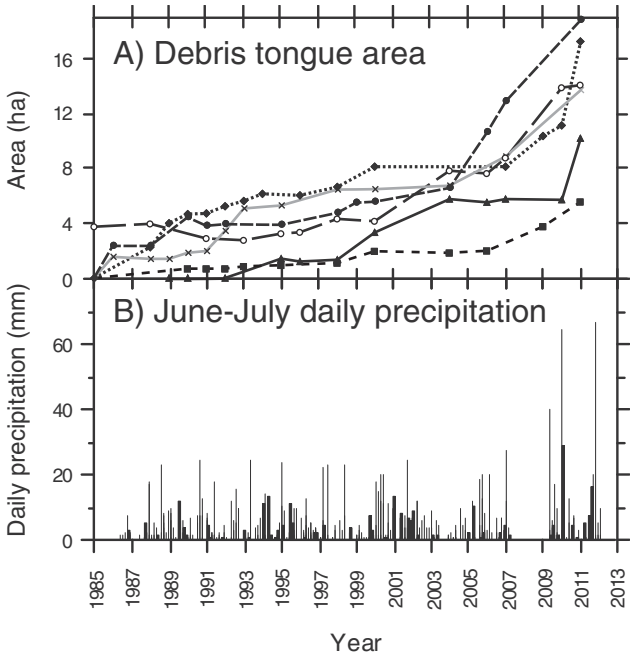

Fig. 8. Debris tongue development and daily June–July precipitation in the Peel Plateau, 1985–2012. A) Debris tongue development was tracked by digitizing disturbance areas on Landsat images from 1985 to 2011. B) June–July daily precipitation at Fort McPherson from 1986 to 2012. Precipitation data is incomplete for 2008 and there are no data for 2009.

14.6 ha, and the majority of the disturbance surface is now devoid of vegetation due to intense mass flow activity (Fig. 6).

Assuming that average headwall height has been at least 10 m, the growth of this slump has displaced well over 2,000,000 m^3 of ice-rich permafrost substrate. Most of the sediments have flowed downslope to form a debris tongue that has infilled the steep sided, V-shaped trunk valley (Figs. 2A, 6 and 10). The deposit extends about 1.5 km down valley and varies in thickness from 3 m to more than 10 m. A transient debris dammed lake developed upstream of this deposit, and has had an area of up to about 5 ha (Fig. 10). Fluvial incision of the debris tongue deposit has periodically caused the lake to drain, and reactivation of the mass flow has blocked the outlet, causing the lake to fill.

The downslope flow of debris from slump FM2 during the extremely wet summer of 2010 exhibited both diurnal and multiday transport pulses indicated by patterns in STIa and STIb (Fig. 11A). In early June, the scar surface was mostly unsaturated and stable due to warm and dry spring conditions. This was followed by numerous medium to high intensity rainfall events, producing the wettest summer on record (Figs. 3 and 7). For the first several weeks of the monitoring period, low magnitude downslope sediment movement was characterized by well-

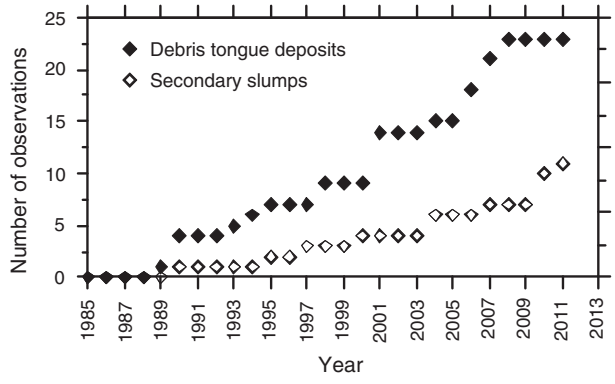

Fig. 9. Chart showing timing of secondary slump and debris tongue development. Data were derived from stacked sequences of Landsat imagery from 1985–2011.

defined pulses of surface flow that lagged diurnal air temperature and net solar radiation peaks by several hours. Diurnal meltwater flooding reworked the deposit surface by multi-threaded channels that carried slurries of mud and rafted debris (Fig. 4B). Some of the lofted blocks of material exceeded 3 m in diameter. On July 4, 2010, the relative magnitude of downslope movements intensified with warm air temperatures and three consecutive days of rainfall totalling 18 mm (Fig. 11A). At peak STIa, the continuous movement of saturated debris extended across the entire 100 m width of the scar surface and maximum rates of downslope movement exceeded 50 m hr^{-1}. The most intense periods of movement were associated with the mobilization and lowering of the entire deposit surface, implying relatively deep-seated, plug-like movement with materials likely sliding over underlying frozen ground. The diurnal patterns of surface flow remained discernable during periods of increased activity when movement continued throughout the 24 hour period. Mass flow activity decreased on July 12, and by July 17 the intensity of movement was comparable with the low levels observed in early summer (Fig. 11A). This decline in the STIa and STIb occurred during the driest period (July 11 to July 22) of the 2010 summer. STI values increased significantly on July 25 following several days of intense rain and warm air temperatures, and remained high until the end of the monitoring period on August 12. A brief decline in transport activity from August 7 to August 9 coincided with a period of lower air temperatures (<12 °C daily max). The final portion of the record captures a rapid mud flow event that swept across the field of view, depositing a mass of material that was gradually reworked within the larger deep-seated mass movement.

FM2 showed similar patterns of sediment transport during the summer of 2012, which was the second wettest summer on record at Fort McPherson (Fig. 3). Camera motion during windy conditions, and vigorous summer vegetation growth in the foreground of the images hampered deriving STIb for 2012, so descriptions here focus on STIa. A slight increase in the daily amplitude of surficial flows occurred with a steady rise in temperatures from June 13 to about June 22. Distinct spikes in STIa between June 25 and 27 followed minor rainfall events, but fluvial activity continued to track the diurnal temperature and solar radiation patterns. The amplitude of diurnal variation was low between June 28 and July 7 despite significant rainfall. This period likely preconditioned the slopes contributing to the major sediment transporting event on July 7–8, which occurred in association with more than 25 mm of rainfall during a 24 hour period (Fig. 11B). Another notable increase in STIa from July 15 to July 19 occurred during a period of slightly lower air temperatures that followed a 40 mm precipitation event. The latter part of July 2012 was characterized by two weeks of dry conditions, moderate air temperatures and lower STI values. Steadily increasing air temperatures towards the end of July and a record 94 mm rainfall event on July 31st stimulated one of the most significant periods of activity in 2012. Although daily temperatures declined after July 31st, elevated rates of continuous mass flow activity with strong diurnal pulses continued for several days. The persistence of warm and dry conditions from August 15, 2012 to the end of the monitoring record was associated with low STI characterized by diurnal flow pulses, similar to the conditions in early summer.

4.4.2. Slump FM3, 2012

Slump FM3 is characterized by a steep chute that connects a low-angle scar zone to the debris tongue and stream (Dempster Creek) in the valley bottom (Figs. 1B and 2C–E). In 2012, the headwall was up to 10 m in height and the scar and debris tongue were 3.8 and 3.2 ha in area, respectively. At this slump a well-defined rill system conveyed meltwater runoff through the stable mass flow deposit (Figs. 2D and 11C). Although there were several intense rainfall events in June and early July 2012, debris from the thawing headwall accumulated in the saturated scar zone. Then on August 3, following a 94 mm rainfall event from July 30–August 1, a surficial mud flow was initiated (Figs. 2E and 11C). From August 3–6, deep-seated transport removed materials

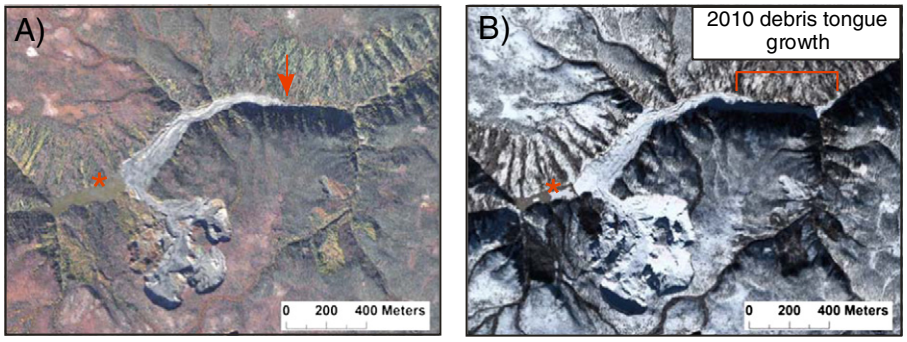

Fig. 10. Quickbird images of slump FM2 from: A) September 2008, and; B) September 2010. Down valley enlargement of the mass flow in 2010 is shown on B). Fieldwork in June and August, 2010 confirmed that mass flow enlargement observed between these two images occurred during summer 2010. The red * indicates the debris dammed lake.

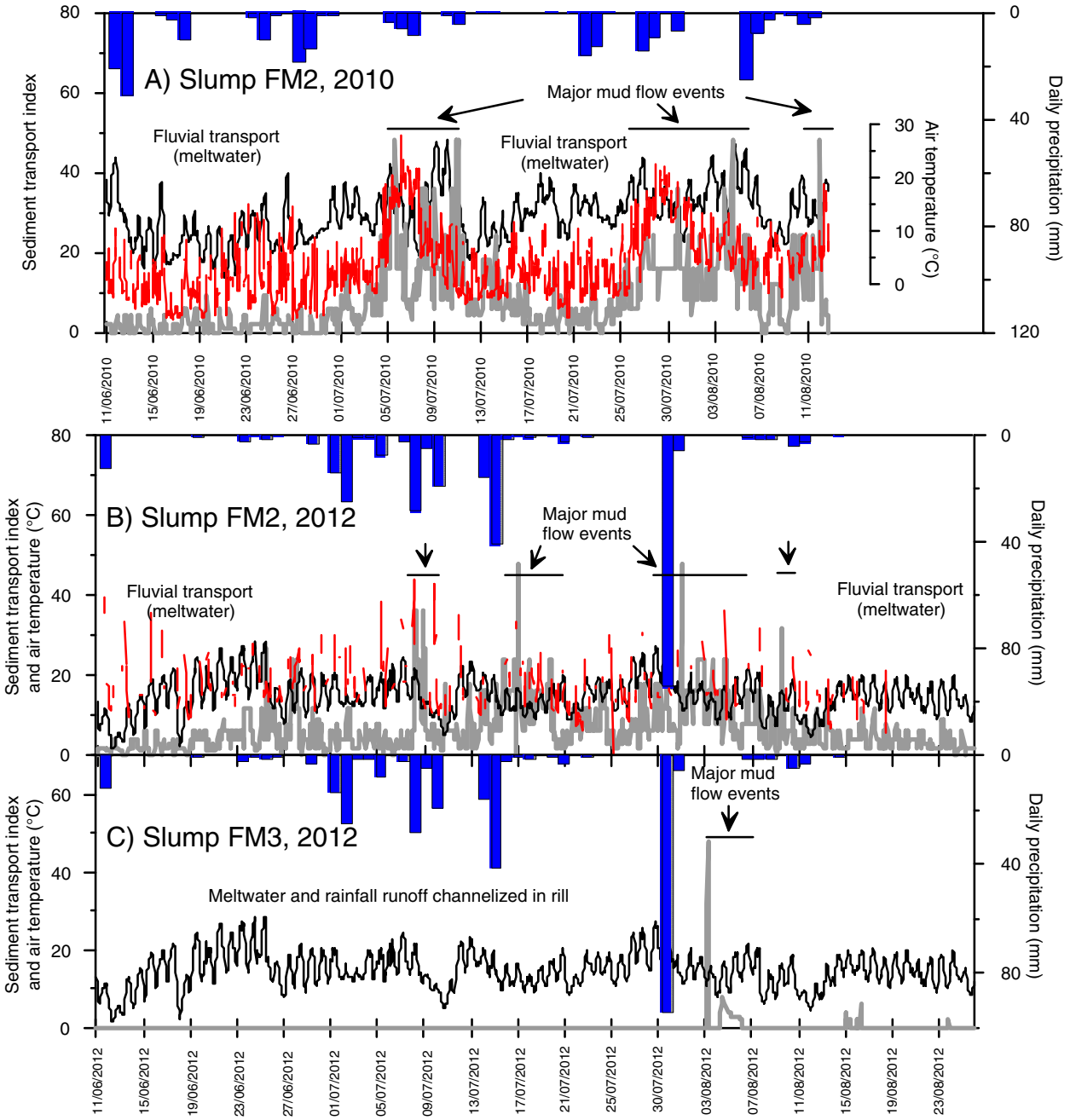

Fig. 11. Time series showing patterns in STIa (grey line), STIb (red line) air temperature (black) and precipitation (blue bars) at: A) FM2 in 2010; B) FM2 in 2012; and C) FM3 in 2012. The STI and temperature data are hourly and precipitation data are daily totals.

from the scar zone. This movement was followed by less intense surficial flow lasting for three days. Ridge development on the lateral edge of the flow and the convex nature of the debris tongue surface indicate that the mass movement was rapid. Minor surface flow events continued to occur sporadically between August 15 and the end of the 2012 monitoring period (Fig. 11C).

4.5. Climate and downslope sediment flux, 2010 and 2012

The summers of 2010 and 2012 were both exceptionally wet. The monitored disturbances experienced significant downslope movement of slumped materials by diurnal, meltwater-driven flows, and periodic deeper-seated mass movements linked to rainfall events that resulted in debris tongue enlargement. The 2010 precipitation total for June–July at Fort McPherson was 201 mm, which exceeded the historical mean by 135 mm (Fig. 3), but the air temperature indices were average (Fig. 7C, D). From June 10 to August 9, 2010, the automated climate station on the Peel Plateau recorded 16 days of rainfall exceeding 10 mm. The frequent rainfall in 2010 contributed to intense mass wasting, including sediment transport by pulses of floodwater, and periods of continuous, deeper-seated mass flows (Fig. 11A). This activity resulted in the net removal of sediment and surface lowering of the FM2 slump scar zone (Fig. 12), and approximately 500 m of down valley debris tongue enlargement (Fig. 10). Quickbird imagery and field reconnaissance confirmed that the debris tongue at slump FM3 was also active and grew approximately 200 m down valley (Fig. 2C). In 2010, there was no significant difference in cumulative 48 hour STIa before and after rainfall, but 48 hour cumulative STIa was elevated following rainfall events on June 25, July 8 and July 28 (Fig. 11A; Table 2). In 2010, sediment transport was highly correlated with variations in hourly air temperature and the smoothed and lagged data suggesting the importance of diurnal and multiday temperature trends in driving meltwater-induced downslope sediment transport (Table 3). STIa was also positively associated with precipitation, but the strongest positive correlations were restricted to precipitation data that was smoothed and lagged at 48 and 96 hour time intervals (Table 3). There was a progressive increase in mean three week STIa through the summer (Table 4).

Summer rainfall in 2012 was also exceptionally high and air temperatures were warmer than 2010 (Fig. 7; Table 4). There were fewer rainy days than in 2010, but several of the precipitation events in 2012 were of extreme magnitude (Fig. 11B). Eight daily rainfall totals exceeded 10 mm, although more than one third of the total precipitation in 2012 fell between July 31 and August 1 (Fig. 11B, C). Mean air temperature and total net radiation were greater in 2012 than in 2010 (Table 4) and there were several periods of up to two weeks in duration with little or no precipitation and low magnitude diurnal pulses of sediment flow (Fig. 11B). The 94 mm rainfall event on July 31, 2012 resulted in a significant increase in mass flow activity at slump FM2 and stimulated the only period of mass flow at slump FM3 (Fig. 11B, C). In 2012, cumulative 48 hour STIa at FM2 was two times greater following rainfall than during the preceding dry periods (Table 2). In 2012 there were significant positive correlations between STIa and antecedent precipitation and air temperature, but overall the strength of the correlations with temperature was much weaker than in 2010. The strongest correlations in 2012 involved the rainfall data smoothed over a 96 hour window length and lagged from 0 to 24 hours (Table 3). The strongest positive correlations between 2012 STIa and air temperature were for data smoothed at 24, 48 and 96 hour window lengths.

Table 2
Mean air temperatures and cumulative STIa, 48 hours pre and post rainfall events for 2010 and 2012. Paired *t*-test was used to compare differences in pre vs. post STIa for 2010 and 2012. Significant differences are indicated in bold.

Date	Event rainfall (mm)	Pre-event temp (°C)	Post-rain temp (°C)	Pre-rain STIa	Post-rain STIa
Summer 2010					
12/6/2010	50	18.4	8.2	68	64
25/6/2010	10.2	11.18	9.65	78	106
8/7/2010	10.1	14.73	15.82	644	932
23/7/2010	13.3	15.34	12.3	223	212
28/7/2010	14.4	18.16	14.63	626	760
7/8/2010	25.2	19.74	10.18	660	260
Cumulative STIa				2299	2334
Mean	20.53	16.26	11.80	383	389
STDev	15.46	3.14	2.99	290	365
Summer 2012					
12/6/2012	12	10.35	8.21	**44**	**89**
2/7/2012	13.8	16.43	13.89	**163**	**200**
9/7/2012	30.8	18.86	10.52	**131**	**337**
16/7/2012	56.7	17.8	13.03	**371**	**758**
31/7/2012	94.3	22.28	14.48	**508**	**774**
Cumulative STIa				1217	2158
Mean	41.52	17.14	12.03	**243**	**432**
STDev	34.54	4.37	2.61	190	318

5. Discussion

5.1. Recent increase in size and frequency of thaw slumps linked to intensification of rainfall

We observed the development of remarkably large thaw slumps on the Peel Plateau that was associated with the progressive thawing of ice-rich permafrost (Fig. 2) (Kokelj et al., 2013; Lacelle et al., 2015). A major increase in number and size of active slumps and debris tongues over the past three decades (Figs. 5 and 6; Table 1) indicate that processes and feedbacks that lead to slump perpetuation have intensified. The acceleration of geomorphic activity has been a recent, regional phenomenon that has occurred with increasing rainfall and no trend in indices of summer air temperature or the occurrence of large-scale landscape disturbance such as fire (Figs. 7 and 8). The development of large debris tongues and an increase in bare slump surfaces suggests

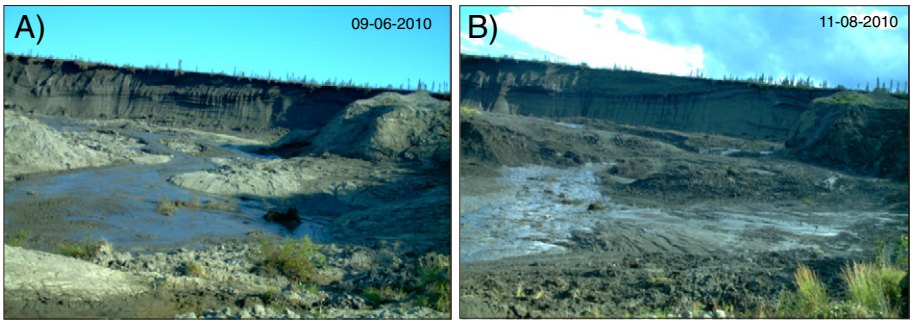

Fig. 12. Headwall, scar zone and upper mass flow of slump FM2 on: A) June 09, 2010, and; B) August 11, 2010. Comparison of the photographs taken from a fixed position shows a lowering of the scar zone following extreme precipitation during summer 2010.

Table 3
Spearman rank correlations between hourly STIa and climate indices for 2010 and 2012. Correlations are between STIa and back-looking cumulative precipitation and running means for net radiation, and air temperature. Smoothed data was based on back looking window lengths (WL) of 12, 24, 48 and 96 hours. The data were also lagged by (Lag) 0, 12, 24, 48, 96 and 192 hour intervals. Three strongest correlations between STIa and each parameter for 2010 and 2012 are indicated in bold. All relationships in bold are significant at $P < 0.001$.

Data	2010			2012		
(Raw and manipulated)	Precip_STIa	ATemp_STIa	NetRad_STIa	Precip_STIa	ATemp_STIa	NetRad_STIa
Precipitation	−0.1213	-	-	-0.0132	-	-
Air temperature	-	0.4659	-	-	0.0786	-
Net radiation	-	-	0.0746	-	-	**0.1128**
WL_Lag_12_0	−0.1273	0.4692	0.1505	0.0180	0.0156	**0.1038**
WL_Lag_12_12	−0.1192	0.4439	−0.0407	0.1636	0.0074	−0.0886
WL_Lag_12_24	−0.1013	0.4395	**0.1848**	0.1409	0.0505	0.0843
WL_Lag_12_48	0.0352	0.3315	0.0839	0.0426	0.1795	0.0774
WL_Lag_12_96	0.0919	0.4105	0.1269	−0.1063	0.1560	0.0877
WL_Lag_12_192	0.0643	0.3283	0.0420	0.1251	0.0324	**0.0985**
WL_Lag_24_0	−0.1245	0.5029	0.1147	0.1007	0.0043	0.0280
WL_Lag_24_12	−0.1071	0.4890	**0.1629**	0.1874	0.0235	0.0073
WL_Lag_24_24	−0.0507	0.4270	0.1530	0.1085	0.0599	0.0070
WL_Lag_24_48	0.0564	0.3631	−0.0265	0.0500	**0.1968**	0.0255
WL_Lag_24_96	0.0967	0.4565	0.0425	−0.0673	0.1645	0.0271
WL_Lag_24_192	0.0222	0.3498	−0.1630	0.1751	0.0308	0.0284
WL_Lag_48_0	−0.0767	0.5075	**0.1795**	0.1374	0.0427	0.0248
WL_Lag_48_12	−0.0353	0.4609	0.1301	0.1441	0.0847	0.0058
WL_Lag_48_24	0.0078	0.4272	0.0789	0.1135	0.1483	0.0198
WL_Lag_48_48	0.1557	0.4454	0.0587	0.0513	**0.2152**	0.0711
WL_Lag_48_96	**0.1711**	**0.5137**	0.0678	0.0286	0.0916	−0.0212
WL_Lag_48_192	−0.0133	0.3229	−0.0847	0.1441	0.0643	0.0035
WL_Lag_96_0	−0.0059	**0.5440**	0.1537	**0.2377**	0.1532	0.0808
WL_Lag_96_12	0.0785	**0.5192**	0.1284	**0.2418**	0.1743	0.0774
WL_Lag_96_24	0.1401	0.5065	0.1017	**0.2080**	**0.1986**	0.0846
WL_Lag_96_48	**0.2228**	0.5119	0.0391	0.1535	0.1895	0.0607
WL_Lag_96_96	**0.3074**	0.5107	−0.0449	0.1301	0.0899	−0.0548
WL_Lag_96_192	0.0034	0.1889	−0.2942	0.0882	0.0931	0.0726

that moisture supplied by rainfall has accelerated scar zone sediment flux (Figs. 8 and 10B), perpetuating slump growth and favouring the development of mega slumps now common on the landscape.

5.2. Patterns and drivers of slump sediment flux

Our fine-scale observations of two slumps indicate that radiation, temperature and precipitation influence diurnal and multiday variations in downslope sediment transport. Temperature-driven ground-ice thaw contributes to diurnal and multiday surface sediment flow pulses, leading to strong correlations between STI and air temperature (Fig. 11A; Table 3). At slump FM2, the threshold for sediment mobilization and downslope flow was exceeded on a daily basis as meltwater from the large massive-ice exposure (Fig. 2B) saturated soils, raising pore-water pressures and causing materials on the gently sloping scar zone to lose cohesion and become entrained (Takahashi, 1981; Costa, 1984). These diurnal meltwater patterns are also evident in runoff, sediment and solute fluxes in streams and rivers below large thaw slumps (Kokelj et al., 2013; Malone et al., 2013).

Table 4
Mean STIa, hourly net radiation and hourly air temperature for 3 week periods in 2010 and 2012. Standard deviation is shown in brackets.

Seasonal prog.	N (days)	Mean STIa	Mean hourly Net Rad (W/m^2)	Mean hourly Air temp (°C)
Summer 2010				
Jun 12–July 1	22	2.00 (0.1)	*145.7* (*7.9*)	10.1 (0.20)
July 2–July 22	21	10.08 (0.39)	134.5 (7.5)	13.5 (0.20)
July 23–Aug. 12	20.5	12.46 (0.36)	116.3 (7.0)	15.1 (0.18)
Summer 2012				
Jun 12–July 1	22	4.04 (0.17)	*196.1* (*9.5*)	15.16 (0.26)
July 2–July 22	21	7.90 (0.30)	135.7 (7.4)	14.55 (0.17)
July 23–Aug. 12	21	8.80 (0.26)	132.9 (7.9)	15.05 (0.22)
Aug. 13–Aug. 26	13.3	3.74 (0.12)	105.0 (9.2)	14.66 (0.17)

Intense or prolonged rainfall is a strong driver of lower frequency, high magnitude mass flow events, which drive debris tongue development (Figs. 6, 8, 10 and 11; Table 2). Ground ice melt maintains high scar-soil moisture levels so that additional water periodically supplied by rainfall can produce episodes of deep-seated, fluidized mass flow when the slump scar zone reaches a critical threshold of saturation (Figs. 2D, E and 11). Accumulated materials supplied by thawing ground ice, slumping, toppling and intermittent translational failures are moderately reworked by diurnal meltwater-induced flows. These materials can be evacuated from the scar zone by the larger, deeper-seated flows that occur at a delayed interval – as much as three days – following major precipitation inputs (Fig. 11A, B, C; Table 2 — 2012). The intensity of these major flow events typically diminishes over the course of several days (Fig. 11). The relative magnitude of downslope sediment transport estimated from field observations suggests that most of the annual sediment flux and debris tongue development can be attributed to the low frequency, high magnitude mass flows.

In 2010, record rainfall was associated with the complete reworking of scar zone materials and major mass flow events at several thaw slumps (Figs. 8, 10 and 11A). Frequent rainfall maintained scar zone slopes and debris tongues in a saturated state, contributing to the overall high rates of downslope sediment movement, the net removal of debris and surface lowering of the scar zone at slump FM2 (Fig. 12) and down valley growth of numerous debris tongues (Figs. 8, 10 and 11). The cumulative effects of several closely spaced rainfall events and the lag in mud flow response likely obscured the geomorphic responses of individual rainfall events in 2010 (Fig. 11A; Table 2).

The importance of high magnitude rainfall events as a driver of major mass flow activity was confirmed by data from summer 2012 when more than two thirds of the rainfall occurred during three high intensity events (Fig. 11B, C). During hot, dry periods, ground ice ablation from the large slump headwalls supplied sufficient moisture to drive diurnal pulses in water, solute and sediment flux (Kokelj et al., 2013), and low magnitude surficial flows. Significant increases in mass flow at

slump FM2 occurred following major rainfall events of 30 mm, 42 mm and 94 mm, respectively (Fig. 11B; Table 2) and the largest rainfall event stimulated the only mass flow activity at FM3 (Figs. 2E and 11C). The strong correlations between smoothed and lagged precipitation with STIa (Table 3) suggests that antecedent and cumulative rainfall is an important driver of the magnitude of surficial flows, as well as the occurrence of low frequency, deep-seated movements.

5.3. Acceleration of mass flow activity perpetuates slump growth leading to larger thaw slumps

The rate and magnitude of sediment transport away from the slump headwall can determine the growth trajectory of a slump. Scar zone sediment flux is influenced by slope, and the sediment and ground ice characteristics of thawing permafrost, giving rise to differences in the growth characteristics of individual disturbances (Fig. 11B, C), and to contrasts in thaw slumps among regions. It is within this geomorphic context that climatic drivers can amplify or diminish the rates and magnitude of sediment evacuation from the slump scar zones, and thereby influence temporal trends in the activity and size of thaw slumps. An increase in the abundance and size of debris tongue deposits (Figs. 5B and 8) indicates an intensification of downslope sediment flux. Our observations strongly suggest that this process has been driven by the recent increase in the frequency and magnitude of rainfall events (Figs. 7, 8 and 11C).

A conceptual model based on our field observations illustrates how an increase in the rate and magnitude of scar zone sediment flux perpetuates slump activity and leads to the development of larger thaw slumps (Fig. 13). The upslope growth potential (d_1) of an active thaw slump is related to headwall height (h), ice content of permafrost (Gi), slope of the undisturbed terrain (*b*-90°) and rate at which debris supplied by ground ice ablation are removed from the toe of the headwall by mass wasting or surface wash (mf_1). General behaviour of the mass flow (mf) is controlled by factors such as sediment texture and slope, which may be considered invariant at our timescale of interest. Temporal variation in the rates and magnitude of scar zone sediment flux is largely driven by soil moisture which is supplied to the scar zone by diurnal ground ice thaw, and by lower frequency rainfall inputs. Our data strongly support the idea that intensification of the rainfall regime has increased the frequency and magnitude of major mass flows (mf_2) and size of downslope debris tongue deposits (Vf_2). Evacuation of sediments from the slump scar zone can help maintain an exposed headwall and increase the upslope growth potential and longevity of the slump ($d_2 > d_1$). The maintenance of larger slump headwalls also intensifies slump activity by increasing rates of retreat (Lacelle et al., 2015), sediment availability and diurnal meltwater contributions. Regional intensification of these processes and feedbacks will perpetuate slump activity resulting in a population of larger disturbances, significant modification of local slopes, enhanced supply of sediments and solutes to downstream environments (Lantuit et al., 2012; Kokelj et al., 2013; Malone et al., 2013) and long-lasting impacts to terrestrial and aquatic ecosystems (Lantz et al., 2009; Mesquita et al., 2010; Thienpont et al., 2013).

6. Conclusions

Based on the analyses and interpretation of our field data we draw the following conclusions:

(1). In the Peel Plateau region, a major increase in number and size of active slump surfaces and debris tongue deposits since the mid-1980s have occurred in concert with a significant increase in the magnitude and intensity of rainfall. There is no trend in summer temperature indices (1986–2010) further supporting the idea that the regional acceleration in thaw slump activity has been driven primarily by increased rainfall.

(2). Air temperature and precipitation interact to influence the moisture regime of slump soils, driving downslope sediment transport from the slump scar zone and debris tongue enlargement. Diurnal pulses in sediment flux indicate that meltwater from thawing ground ice can induce high frequency, low magnitude surficial-sediment flow. Strong relationships between air temperature and flow events were observed at diurnal and multiday scales in summer of 2010 when frequent rainfall maintained slopes in a saturated condition.

(3). Rainfall can elevate scar zone soil moisture conditions, reducing soil strength and stimulating major mass flows. These lower-frequency high magnitude flows evacuate sediments that would otherwise accumulate in the slump scar zone. The acceleration of scar zone sediment flux can help maintain a headwall of exposed ground ice and inhibit slump stabilization. This process can perpetuate slump growth leading to the development of larger thaw slumps and debris tongue deposits. Feedbacks resulting in changes to stream base-level can enhance valley-side erosion and initiate additional slumping on adjacent slopes.

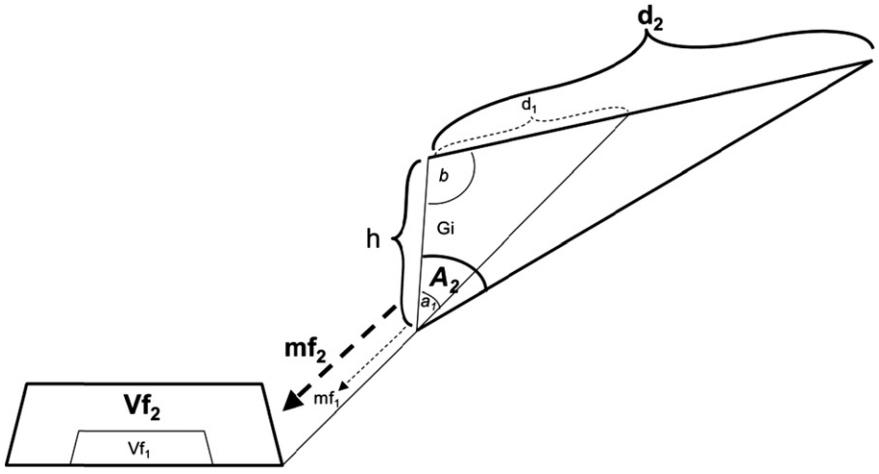

Fig. 13. Conceptual model illustrating the impact of increased mass flow activity (mf) and removal of materials from the slump headwall on development of valley debris tongue deposits (Vf) and upslope growth potential of the slump (d). h indicates headwall height at a given point in time and Gi is ground ice content and *b*-90° is the approximate slope of the undisturbed terrain. Upslope growth potential of the slump (d) is constrained by h, Gi and *b*-90°. This relationship can be modified by varying mf. An increase in mf (mf_2) will maintain greater headwall height (h) with upslope retreat to perpetuate slump growth and produce a larger disturbance.

(4). Intensification of rainfall regimes can rapidly destabilize ice-rich, fluvially incised, moraine dominated landscapes. These geomorphically-sensitive permafrost environments are susceptible to thaw slumping, occur across the circumpolar North and constitute major sediment sources for many rivers and coastal zones. The development of larger slumps can have significant and enduring consequences on slope and fluvial geomorphology, and downstream ecosystems.

Acknowledgements

This work was supported by the NWT Cumulative Impact Monitoring Program, the Aurora Research Institute and the NWT Geoscience Office, Government of the Northwest Territories, by Natural Sciences and Engineering Research Council of Canada grants to D. Lacelle and T. Lantz, and by the Polar Continental Shelf Project. Institutional support from the Gwich'in Tribal Council, Gwich'in Renewable Resources Board and the Tetlit Gwich'in Renewable Resources Council is gratefully acknowledged. We thank Shawne Kokelj and Meg McCluskie from Water Research and Studies, Environment and Natural Resources, Government of the Northwest Territories for supplying data from the Peel Plateau Meteorological Station. The authors thank Kyle Rentmeister from the NWT Centre for Geomatics for the GIS work. Jaya Bastedo, Steven Tetlichi, Clifford Vaneltsi, Gina Vaneltsi and Billy Wilson supplied critical field and logistical support. We thank Larry Flysak, Environment Canada, for timely provision of unpublished Fort McPherson Airport precipitation data. Comments by two anonymous reviewers have improved the clarity of this manuscript. NWT Geoscience contribution 87.

References

Alexanderson, H.L., Adrielsson, L., Hjort, C., Möller, P., Antonov, O., Eriksson, S., Pavlov, M., 2002. Depositional history of North Taymyr ice-marginal zone, Siberia – a landsystem approach. J. Quat. Sci. 17, 361–382.

Astakhov, V.I., Kaplyanskaya, F.A., Tarnogradsky, V.D., 1996. Pleistocene permafrost of West Siberia as a deformable glacier bed. Permafr. Periglac. 7, 165–191.

Bjornson, J., 2003. Les glissements retrogressifs de fonte de la riviere Willow, Territoires du Nord-Ouest, Canada: caractéristiques sedimentologiques, distribution spatiale et temporelle. (MSc. thesis). University of Ottawa, Ottawa, Canada.

Brooker, A., Fraser, R., Olthoff, I., Kokelj, S.V., Lacelle, D., 2014. Mapping the activity and evolution of retrogressive thaw slumps by Tasseled Cap trend analysis of a Landsat satellite image stack. Permafr. Periglac. 25, 243–256.

Burn, C.R., Kokelj, S.V., 2009. The permafrost and environment of the Mackenzie Delta area. Permafr. Periglac. 20, 83–105.

Burn, C.R., Lewkowicz, A.G., 1990. Retrogressive thaw slumps. Can. Geogr. 34, 273–276.

Callaghan, T.V., Johansson, M., Anisimov, O., Christiansen, H.H., Instanes, A., Romanovsky, V., Smith, S., 2011. Changing permafrost and its impacts. In Snow, Water, Ice and Permafrost in the Arctic (SWIPA): Climate Change and the Cryosphere. Arctic Monitoring and Assessment Programme (AMAP), Oslo, Norway (Chapter 5).

Catto, N.R., 1996. Richardson Mountains, Yukon-Northwest Territories: the northern portal of the postulated 'ice-free corridor'. Quat. Int. 32, 3–19.

Cogley, J.G., McCann, S.B., 1976. An exceptional storm and its effects in the Canadian High Arctic. Arct. Alp. Res. 8, 111–114.

Costa, J.E., 1984. Physical Geomorphology of Debris Flows. Developments and Applications of Geomorphology, pp. 268–317 (Chapter 9).

Duk-Rodkin, A., Hughes, O.L., 1992a. Surficial Geology, Fort McPherson - Bell River, Yukon-Northwest Territories. Geological Survey of Canada (Map 1754A).

Duk-Rodkin, A., Hughes, O.L., 1992b. Surficial Geology, Trail River – Eagle River, Yukon-Northwest Territories. Geological Survey of Canada (Map 1744A).

Environment Canada, 2012. National Climate Data and Information Archive, Fort McPherson, NWT. http://climate.weatheroffice.gc.ca.

Fortier, D., Allard, M., Shur, Y., 2007. Observation of rapid drainage system development by thermal erosion of ice wedges on Bylot Island, Canadian Arctic Archipelago. Permafr. Periglac. 18, 229–243.

Fulton, R.J.,(compiler) 1995. Surficial materials of Canada. Geological Survey of Canada, Map 1880A, scale 1:500,000.

Grom, J.D., Pollard, W.H., 2008. A study of high Arctic retrogressive thaw slump dynamics, Eureka Sound Lowlands, Ellesmere Island. In: Kane, D.L., Hinkel, K.M. (Eds.), Proceedings of the Ninth International Conference on Permafrost. Institute of Northern Engineering, University of Alaska, Fairbanks, Alaska, pp. 545–550.

Hirsch, R.M., Slack, J.R., Smith, R.A., 1982. Techniques of Trend Analysis for Monthly Water-Quality Data. Water Resour. Res. 18, 107–121.

Jorgenson, M.Y., Shur, Y.L., Osterkamp, T.E., 2008. Thermokarst in Alaska. Proceedings of the Ninth International Conference on Permafrost. In: Kane, D.L., Hinkel, K.M. (Eds.), Institute of Northern Engineering, University of Alaska, Fairbanks, Alaska, pp. 869–876.

Judge, A.S., 1973. The thermal regime of the Mackenzie Valley: Observations of the natural state; Environmental Social Committee Northern Pipeline (Canada). Task Force on Northern Oil Development Report 73-38 (177 pp.).

Kokelj, S.V., Jorgenson, T., 2013. Advances in thermokarst research. Permafr. Periglac. 24, 108–119.

Kokelj, S.V., Lacelle, D., Lantz, T.C., Tunnicliffe, J., Malone, L., Clark, I.D., Chin, K., 2013. Thawing of massive ground ice in mega slumps drives increases in stream sediment and solute flux across a range of watershed scales. J. Geophys. Res. Earth 118, 681–692. http://dx.doi.org/10.1002/2013jgrf.20063.

Kokelj, S.V., Lantz, T.C., Wolfe, S.A., Kanigan, J.C., Morse, P.D., Coutts, R., Molina-Giraldo, N., Burn, C.R., 2014. Distribution and activity of ice wedges across the forest tundra transition, western Arctic Canada. J. Geophys. Res. Earth 119, 2032–2047. http://dx.doi.org/10.1002/2014jgrf.003085.

Lacelle, D., Bjornson, J., Lauriol, B., 2010. Climatic and geomorphic factors affecting contemporary (1950–2004) activity of retrogressive thaw slumps on the Aklavik Plateau, Richardson Mountains, NWT, Canada. Permafr. Periglac. 21, 1–15.

Lacelle, D., Lauriol, B., Zazula, G., Ghaleb, B., Utting, N., Clark, I.D., 2013. Timing of advance and basal condition of the Laurentide Ice Sheet during the last glacial maximum in the Richardson Mountains, NWT. Quat. Res. 80, 274–283.

Lacelle, D., Brooker, A., Fraser, R.H., Kokelj, S.V., 2015. Distribution and growth of thaw slumps in the Richardson Mountains – Peel Plateau region, northwestern Canada. Geomorphology 235, 40–51. http://dx.doi.org/10.1016/j.geomorph.2015.01.024.

Lafrenière, M.J., Lamoureux, S.F., 2013. Thermal perturbation and rainfall runoff have greater impact on seasonal solute loads than physical disturbance of the active layer. Permafr. Periglac. 24, 241–251.

Lakeman, T.R., England, J.H., 2012. Paleoglaciological insights from the age and morphology of the Jesse moraine belt, western Canadian Arctic. Quat. Sci. Rev. 47, 82–100.

Lamoureux, S.F., Lafrenière, M.J., 2009. Fluvial impact of extensive active layer detachments, Cape Bounty, Melville Island, Canada. Arct. Antarct. Alp. Res. 4, 59–68.

Lantuit, H., Pollard, W.H., 2008. Fifty years of coastal erosion and retrogressive thaw slump activity on Herschel Island, southern Beaufort Sea, Yukon Territory, Canada. Geomorphology 95, 84–102.

Lantuit, H., Pollard, W.H., Couture, N., Fritz, M., Schirrmeister, L., Meyer, H., Hubberten, H.-W., 2012. Modern and late Holocene retrogressive thaw slump activity on the Yukon coastal plain and Herschel Island, Yukon Territory, Canada. Permafr. Periglac. 23, 39–51.

Lantz, T.C., Kokelj, S.V., 2008. Increasing rates of retrogressive thaw slump activity in the Mackenzie Delta region, N.W.T. Canada. Geophys. Res. Lett. 35, L06502.

Lantz, T., Kokelj, S.V., Gergel, S.E., Henry, G.H., 2009. Relative impacts of disturbance and temperature: persistent changes in microenvironment and vegetation in retrogressive thaw slumps. Glob. Chang. Biol. 15, 1664–1675.

Lewkowicz, A.G., 1987. Headwall retreat of ground-ice slumps, Banks Island, Northwest Territories. Can. J. Earth Sci. 24, 1077–1085.

Lewkowicz, A.G., Harris, C., 2005. Morphology and geotechnique of active-detachment failures in discontinuous and continuous permafrost, northern Canada. Geomorphology 69, 275–297.

Lewkowicz, A.G., Kokelj, S.V., 2002. Slope sediment yield in arid lowland continuous permafrost environments, Canadian Arctic Archipelago. Catena 46, 261–283.

Mackay, J.R., 1967. Permafrost depths, Lower Mackenzie Valley, Northwest Territories. Arctic 20, 21–26.

Malone, L., Lacelle, D., Kokelj, S.V., Clark, I.D., 2013. Impacts of hillslope thaw slumps on the geochemistry of permafrost catchments (Stony Creek watershed, NWT, Canada). Chem. Geol. 356, 38–49. http://dx.doi.org/10.1016/j.chemgeo.2013.07.010.

McRoberts, E.C., Morgenstern, N.R., 1974. The stability of thawing slopes. Can. Geotech. J. 11, 447–469.

Mesquita, P.S., Wrona, F.J., Prowse, T.D., 2010. Effects of retrogressive permafrost thaw slumping on sediment chemistry and submerged macrophytes in Arctic tundra lakes. Freshw. Biol. 55, 2347–2358.

Murton, J.B., 2001. Thermokarst sediments and sedimentary structures, Tuktoyaktuk Coastlands, western Arctic Canada. Glob. Planet. Chang. 28, 175–192.

Norris, D.K., 1984. Geology of the northern Yukon and northwestern District of Mackenzie. Geological Survey of Canada, Map 1581A, scale 1:500 000.

O'Neill, H.B., Burn, C.R., Kokelj, S.V., Lantz, T.C., 2015. "Warm" tundra: atmospheric and near-surface ground temperature inversions across an alpine tree line in continuous permafrost, western Arctic, Canada. Permafr. Periglac. http://dx.doi.org/10.1002/ppp.1838 (in press).

Rampton, V.N., 1982. Quaternary geology of the Yukon Coastal Plain. Geol. Surv. Can. Bulletin 317.

Romanovsky, V.E., Smith, S.L., Christiansen, H.H., 2010. Permafrost thermal state in the polar Northern Hemisphere during the International Polar Year 2007-2009: a synthesis. Permafr. Periglac. 21, 106–116.

St-Onge, D.A., McMartin, I., 1999. The Bluenose Lake Moraine, a moraine with a glacier core. Géog. Phys. Quatern. 53, 287–296.

Takahashi, T., 1981. Debris flows. Annu. Rev. Fluid Mech. 13, 57–77.

Thienpont, J.R., Rühland, K.M., Pisaric, M.F.J., Kokelj, S.V., Kimpe, L.E., Blais, J.M., Smol, J.P., 2013. Biological responses to permafrost thaw slumping in Canadian Arctic lakes. Freshw. Biol. 58, 337–353.

Walsh, J.E., Overland, J.E., Groisman, P.Y., Rudolf, B., 2011. Arctic Climate: Recent Variations. In Snow, Water, Ice and Permafrost in the Arctic (SWIPA): Climate Change and the Cryosphere. Arctic Monitoring and Assessment Programme (AMAP), Oslo, Norway (Chapter 2).